Inorg. Chem. **2006**, *45*, 3746–3755

Synthesis, X-ray Crystal Structures, Magnetism, and Phosphate Ester Cleavage Properties of Copper(II) Complexes of N-Substituted Derivatives of 1,4,7-Triazacyclononane

Matthew J. Belousoff, Martin B. Duriska, Bim Graham, Stuart R. Batten, Boujemaa Moubaraki, Keith S. Murray, and Leone Spiccia*

School of Chemistry, Monash University, Victoria, 3800, Australia

Received November 16, 2005

Two new N-substituted derivatives of the 1,4,7-triazacyclononane (tacn) macrocycle, 1-benzyl-4,7-dimethyl-1,4,7-triazacyclononane (L^2) and 1,4,7-tris(3-cyanobenzyl)-1,4,7-triazacyclononane (L^3), have been prepared and, together with 1,4-dimethyl-1,4,7-triazacyclononane (L^1), have been used to synthesize the corresponding hydroxo-bridged binuclear copper (II) complexes, $[Cu_2(\mu\text{-}OH)_2L_2](ClO_4)_2 \cdot xH_2O$ (**1** L = L^1, $x = 0$; **2** L = L^2, $x = 1$; **3** L = L^3, $x = 2$). The X-ray crystal structures of all three complexes reveal the presence of $[Cu_2(\mu\text{-}OH)_2]^{2+}$ cores capped by pairs of facially coordinating tacn ligands so that the Cu(II) centers reside in distorted square pyramidal coordination environments. Variable-temperature magnetic susceptibility measurements indicate weak antiferromagnetic coupling ($J = -36.4$ cm^{-1}) between the Cu(II) centers in **1**, while the centers in **2** and **3** have been shown to interact ferromagnetically ($J = 11.2$ and 49.3 cm^{-1}, respectively). The variation in the strength and sign of these interactions has been rationalized in terms of the differing geometries of the $[Cu_2(\mu\text{-}OH)_2]^{2+}$ cores. The ability of the Cu(II) complexes to cleave phosphate ester bonds has been probed using the model phosphate ester bis(4-nitrophenyl)-phosphate (BNPP) at pH 7.4 and a temperature of 50 °C. The measured rate constant for **3** (3×10^{-4} s^{-1}) is significantly greater than those previously reported for the Cu(II) complexes of the fully alkylated tacn ligands, Me_3tacn and $^i Pr_3$tacn, which until now have been rated as the most effective tacn-based phosphate ester cleavage agents.

Introduction

Phosphate ester bonds are an integral part of biological systems, with both RNA and DNA containing sugar−phosphate backbones with phosphodiester linkages. Such bonds are extremely resistant to hydrolysis with long cleavage half-lives at neutral pH and 25 °C.[1] To sustain life, nature uses an array of metalloenzymes to enhance the rate of phosphate ester cleavage. A prominent feature of many of these phosphatases is the presence of one or more coordinated metal centers at their active sites, which carry out the cleavage of phosphate esters through the nucleophilic attack of the bound, electrophillically activated substrate by a metal-bound hydroxide group.

The design and synthesis of simple metal complexes that function as "artificial phosphatases" is a very active area of research that can provide important insights into the relationship between structure and activity for the natural enzymes. Such complexes may also find potential application as tools in molecular biology or as pharmaceutical agents. By tethering the complexes to oligonucleotide strands, there is the potential to develop new "antisense" therapeutics that possess the ability to not only bind to target DNA/RNA sequences but also to cleave the phosphate ester bonds contained therein.[2−5]

Among the various model complexes that have been described in the literature, the copper(II) complexes of a number of ligands incorporating the 1,4,7-triazacyclononane (tacn) macrocycle have been shown to hydrolyze phosphate esters at reasonably fast rates. One pertinent observation has been that simple alkylation of all three nitrogen atoms of

* To whom correspondence should be addressed. Fax: +61 3 99054597. Tel: +61 3 99054526. E-mail: leone.spiccia@sci.monash.edu.au.

(1) Fry, F.; Fischmann, A. J.; Belousoff, M. J.; Spiccia, L.; Brugger, J. *Inorg. Chem.* **2005**, *44*, 941.
(2) Zelder, F. H.; Mokhir, A. A.; Kramer, R. *Inorg. Chem.* **2003**, *42*, 8618.
(3) Hegg, E. L.; Burstyn, J. N. *Inorg. Chem.* **1996**, *35*, 7474−7481.
(4) Hegg, E. L.; Burstyn, J. N.; Deal, K. A.; Kiessling, L. L. *Inorg. Chem.* **1997**, *36*, 1715.
(5) Hegg, E. L.; Burstyn, J. N. *Coord. Chem. Rev.* **1998**, *173*, 133.

10.1021/ic051983+ CCC: $33.50
Published on Web 03/28/2006

the tacn ring leads to complexes with significantly enhanced activity. In a quest to develop even more efficient systems, we have therefore been investigating the effects that different types and degrees of N-substitution have on the rates of phosphate ester cleavage.

Another area of continuing interest is the development of an understanding of magnetic interactions in bridged metal complexes. The magnetic properties of copper(II) complexes, in particular, have been widely studied since the 1970s, and efforts have been made to develop structure−activity relationships which rationalize the coupling between the Cu(II) centers in hydroxo-bridged complexes.[6,7] Recent advances in computational chemistry, such as density funtional theory, have led to new efforts to gain new insight into how the molecular structure influences the magnetic interactions between metal centers,[8] including hydroxo-bridged copper(II) dimers.[9] Copper(II) complexes of tacn derivatives have attracted much attention in this regard, with the vast majority of the systems reported to date exhibiting antiferromagnetic exchange interactions.[10−13] Two of the complexes reported herein are unusual in this family of tacn complexes in that the coupling between the two hydroxo-bridged Cu(II) centers is ferromagnetic.

This paper reports the synthesis of two new derivatives of 1,4,7-triazacyclononane (viz., 1-benzyl-4,7-dimethyl-1,4,7-triazacyclononane (L^2) and 1,4,7-tris(3-cyanobenzyl)-1,4,7-triazacyclononane (L^3)) and their use in the preparation of "roof-shaped" hydroxo-bridged copper(II) complexes, in which the $[Cu_2(\mu\text{-}OH)_2]^{2+}$ core is asymmetric and the two Cu-tacn moieties adopt a syn configuration across the hydroxo-bridged core. We also report the synthesis of the corresponding complex formed by 1,4-dimethyl-1,4,7-triazacyclononane (L^1) in which the $[Cu_2(\mu\text{-}OH)_2]^{2+}$ core is symmetric and the Cu-tacn moieties are in an anti configuration**.** The magnetic properties of the three complexes have been investigated and conclusions reached about the dependence of magnetic exchange interactions on the structure of the $[Cu_2(\mu\text{-}OH)_2]^{2+}$ core. Finally, we report on the ability of these complexes to cleave phosphate esters, which has involved the study of the reaction of the complexes with the model phosphate ester, bis(nitrophenyl)phosphate (BNPP).[1,14−19]

Experimental Section

All solvents used were reagent or analytical grade and were used as purchased. Distilled H_2O was used throughout. Acetonitrile was predried over 4 Å sieves. Chloroform was HPLC grade and was used as purchased. THF was dried with sodium and then distilled from Na/benzophenone and used immediately. 1,4-Dimethyl-1,4,7-triazacyclononane (L^1) was prepared by a procedure reported by Wieghardt and co-workers.[20,21]

Instrumentation and Methods. TLC was performed using silica gel 60 F-254 (Merck) plates with detection of species present by UV or $KMnO_4$ spray. Concentrations were performed under reduced pressure at 50 °C (water bath). ^1H and ^{13}C NMR spectra were recorded at 25 °C in D_2O or $CDCl_3$ (as listed) using Bruker or Varian Spectrometers (200, 300, or 400 MHz instruments). Spectra were calibrated using TMS as an internal standard. UV−vis spectra were recorded on 0.01−10 mM solutions in quartz cuvettes using Varian Cary 3 or 5G spectrophotometers. IR spectra were recorded using a Perkin-Elmer FTIR 1600 series spectrometer at 4.0 cm^{-1} resolution, using KBr disks. Cation-exchange column chromatography was performed using Sephadex SP C25 columns with a 30 mm diameter. Mass spectra were recorded using a Micromass Platform II, with an ESI source. The capillary voltage was set at 3.5 eV and the cone voltage at 35 V. CHN microanalysis was perfomed by the Campbell Microanalytical Laboratory, University of Otago, New Zealand. Magnetic susceptibilities were measured on 20 mg samples using a Quantum Design MPMS 5 Squid instrument. Diamagnetic corrections were made for the gelatine capsule holder and for ligands, the latter using Pascal's constants.

Caution: Although no problems were encountered in this work, transition metal perchlorates are potentially explosive and should be prepared in small quantities and handled with care.

Syntheses. *N,N′*-Bis(2-chloroacetyl)-*N,N′*-dimethylethylenediamine. The synthesis was adapted from that described by Lin et al.[22] *N,N′*-Dimethylethylenediamine (8.00 g, 91 mmol) and K_2CO_3 (25.08 g, 0.18 mol) were dissolved in dry $CHCl_3$ (200 mL) and stirred at 0 °C under N_2. To this mixture, a solution of chloroacetylchloride (20 g, 0.18 mol) in dry $CHCl_3$ (10 mL) was added dropwise. The mixture was stirred for 2 h, and then it was heated at reflux for a further 2 h. The reaction mixture was allowed to cool room temperature and then washed with H_2O (3 × 100 mL). The organic phase was dried with $MgSO_4$, and the solvent was removed under reduced pressure to yield the crude product as a white solid. Yield: 16.79 g, 77%. The product was recrystallized in CH_2Cl_2 and hexane to give crystals suitable for X-ray diffraction. mp: 124 °C. ESI-MS: 241.4 $[M + H]^+$. ^1H NMR ($CDCl_3$): δ 3.12 (s, 6H, N−CH_3), 3.61 (s, 4H, CH_2−N), 4.05 (s, 4H, CH_2−Cl). ^{13}C NMR ($CDCl_3$): δ 36.09, 41.40, 45.27, 167.40. Selected IR bands (Nujol, cm^{-1}): ν 3295 s, 1651 s br, 1416 s, 1310s, 1276s, 1203w, 1176s, 1105s, 982w, 942w, 723w, 668w.

1,4-Dimethyl-7-benzyl-1,4,7-triazacyclononane-2,6-diamide. This synthesis was adapted from that used by Grenz et al. to prepare other tacn-diamides.[23] *N,N′*-Bis(2-chloroacetyl)-*N,N′*-dimethylethylenediamine (4.00 g, 16.7 mmol), LiBr (3.02 g, 35.1 mmol), and

(6) Crawford, V. H.; Richardson, H. W.; Wasson, J. R.; Hodgson, D. J.; Hatfield, W. E. *Inorg. Chem.* **1976**, *15*, 2107.
(7) Charlot, M. F.; Jeannin, S.; Kahn, O.; Lucrece-Abaul, J. *Inorg. Chem.* **1979**, *18*, 1675.
(8) Hu, H.; Liu, Y.; Zhang, D.; Liu, C. *THEOCHEM* **2001**, *546*, 73.
(9) Ruiz, E.; Alemany, P.; Alvarez, S.; Cano, J. *J. Am. Chem. Soc.* **1997**, *119*, 1297.
(10) Wieghardt, K.; Chaudhuri, P.; Ventur, D.; Peters, E.-M.; Peters, K.; Simon, A. *Angew. Chem., Int. Ed. Engl.* **1985**, *24*, 1985.
(11) Farrugia, L. J.; Lovatt, P. A.; Peacock, R. D. *J. Chem. Soc., Dalton Trans.* **1997**, 911.
(12) Graham, B.; Hearn, M. T. W.; Junk, P. C.; Kepert, C. M.; Mabbs, F. E.; Moubaraki, B.; Murray, K. S.; Spiccia, L. *Inorg. Chem.* **2001**, *40*, 1536.
(13) Graham, B.; Spiccia, L.; Fallon, G. D.; Hearn, M. T. W.; Mabbs, F. E.; Moubaraki, B.; Murray, K. S. *J. Chem. Soc., Dalton Trans.* **2002**, 1226.
(14) Iranzo, O.; Richard, J. P.; Morrow, J. R.; Elmer, T. *Inorg. Chem.* **2003**, *42*, 7737.
(15) Hegg, E. L.; Mortimore, S. H.; Cheung, C. L.; Huyett, J. E.; Powell, D. R.; Burstyn, J. N. *Inorg. Chem.* **1998**, *38*, 2691.
(16) Burstyn, J. N.; Deal, K. A. *Inorg. Chem.* **1993**, *32*, 3585.
(17) Iranzo, O.; Richard, J. P.; Morrow, J. R.; Kovalevsky, A. Y. *J. Am. Chem. Soc.* **2003**, *125*, 1988.
(18) Fry, F. H. Ph.D. Thesis, Monash University, Victoria, Australia 2002.
(19) Vichard, C.; Kaden, T. A. *Inorg. Chim. Acta* **2002**, *337*, 173.
(20) Flassbeck, C.; Wieghardt, K. *Z. Anorg. Allg. Chem.* **1992**, *608*, 60.
(21) Halfen, J. A.; Tollman, W. B.; Wieghardt, K. *Inorg. Synth.* **1998**, *32*, 75.
(22) Lin, W. O.; Figueira, J. A. A.; Alt, H. G. *Monatsh. Chem.* **1985**, *116*, 217.
(23) Grenz, A.; Ceccarelli, S.; Bolm, C. *Chem. Commun.* **2001**, 1726.

Na_2CO_3 (15.83 g, 0.15 mol) were added to MeCN (250 mL). The mixture was then heated to reflux with stirring under N_2. Once the solution was at reflux, a solution of benzylamine (1.81 mL, 16.9 mmol) in MeCN (60 mL) was added dropwise, and the reaction mixture was heated for a further 21 h. It was then cooled to room temperature and filtered through Celite, and the solvent was removed under vacuum. The resulting oil was dissolved in MeOH and then run through a plug of neutral alumina. The solvent was again removed under vacuum, and the oil was then purified by column chromatography (Merck Silica Gel 60; eluent CH_2Cl_2/MeOH, 9/1 v/v). The desired product had an R_f of 0.49. Yield: 1.82 g, 40%. ESI-MS: 276.3 $[M+H]^+$, 298.3 $[M + Na]^+$, 551.4 $[2M]^+$, 572.9 $[2M + Na]^+$. ^{1}H NMR ($CDCl_3$): δ 2.97 (s, 6H, N−CH_3), 3.39 (s, 4H, tacn ring CH_2), 3.73 (s, 2H, benzyl CH_2), 3.80 (s, 4H, tacn ring CH_2), 7.25−7.34 (m, 5H, aromatic CH). ^{13}C NMR ($CDCl_3$): δ 37.73, 49.94, 58.52, 61.36, 127.85, 128.75, 129.60, 137.23, 170.11.

1,4-Dimethyl-7-benzyl-1,4,7-triazacyclononane (L^2). The diamide (1.816 g, 6.60 mmol) was dissolved in THF (100 mL), and the solution heated to reflux under N_2. $LiAlH_4$ (2.51 g, 66.0 mmol) was added to this mixture, and it was refluxed for a further for 17.5 h. The mixture was then cooled to 0 °C in an ice water bath, and water was added very slowly to react with the excess $LiAlH_4$. It was then filtered to remove the white precipitate, and the filtrate was concentrated under high vacuum. The oily product was dissolved in $CHCl_3$ and dried over $MgSO_4$, and then the solvent was evaporated to yield the product as a clear oil. Yield: 1.6 g, 98%. ESI-MS: 248.3 $[M + H]^+$, 266.3 $[M + NH_4]^+$. ^{1}H NMR ($CDCl_3$): δ 2.35 (s, 6H, N−CH_3), 2.73 (s, 8H, tacn ring CH_2), 2.91 (s, 4H, tacn ring CH_2), 3.65 (s, 2H, benzyl CH_2), 7.25−7.32 (m, 5H, benzene ring CH). ^{13}C NMR ($CDCl_3$): δ 34.08, 35.78, 37.91, 50.06, 58.77, 61.60, 128.03, 128.92, 129.77. Selected IR bands (neat, cm^{-1}): ν 2977s, 2812s, 2227w, 1693s, 1556s, 1454s, 1157s, 1097w, 1068w, 1031w, 998s, 992w, 858s, 771s, 683w, 678s. UV−vis (EtOH) λ_{max} (ϵ_{max}): 206 nm (4490 M^{-1} cm^{-1}).

1,4,7-Tris(3-cyanobenzyl)-1,4,7-triazacyclononane (L^3). tacn·3HCl (1 g, 4.2 mmol) was dissolved in 40 mL of water, and then 3-cyanobenzylbromide (2.9 g, 14.8 mmol) was added. NaOH (3 g, 75 mmol) dissolved in water (5 mL) was slowly added to this mixture, and the reaction mixture was stirred at room temperature for 16 h. The yellow oil was separated from the aqueous layer and dissolved in dichloromethane. After the product was washed with water and dried over $MgSO_4$, evaporation yielded the desired product as a yellow oil. Yield: 1.32 g, 66%. ESI-MS: 475.4 $[M + H]^+$. ^{1}H NMR ($CDCl_3$): δ 7.62−7.40 (m, 12H, aromatic CH), 3.64 (s, 6H, Bz−CH_2), 2.78 (s, 12H, tacn ring CH_2). ^{13}C NMR ($CDCl_3$ (MeOH)): δ 54.71, 55.93, 61.89, 111.94, 118.12, 129.05, 130.36, 133.328, 145.27. Selected IR bands (KBr disk, cm^{-1}): ν 2924m, 2228s, 1618m, 1431m, 1064m. UV−vis (EtOH) λ_{max} (ϵ_{max}): 282 (3130), 274 (3470), 224 (34 500), 206 nm (36 900 M^{-1} cm^{-1}).

$[Cu_2(\mu_2\text{-}OH)_2L^1_2](ClO_4)_2$ (1). A solution of $CuCl_2\cdot 2H_2O$ (0.217 g, 1.28 mol) in H_2O (6 mL) was added to a solution of L^1 (0.10 g, 0.64 mmol) in H_2O (5 mL). The pH was adjusted to 9 by the addition of 2 M NaOH. The solution was then filtered to removed insoluble copper hydroxide, and $NaClO_4$ (0.2 g) was added to the filtrate. The resulting solution was slowly evaporated to yield deep blue crystals. Yield: 0.59 g, 69%. Diffusion of Et_2O into a MeCN solution of the complex yielded crystals suitable of X-ray diffraction. Anal. Calcd for $C_{16}H_{40}Cl_2Cu_2N_6O_{10}$: C, 28.5; H, 6.0; N, 12.5. Found: C, 28.4; H, 6.0; N, 12.4. Selected IR bands (KBr disk, cm^{-1}): ν 2923s, 2869s, 2815w, 1654w, 1638w, 1560s, 1524w, 1458s, 1143s, 1118s, 1089s, 819w. UV−vis spectrum (H_2O) λ_{max} (ϵ_{max}): 624 (86), 260 nm (5260 M^{-1} cm^{-1}).

$[Cu_2(\mu_2\text{-}OH)_2L^2_2](ClO_4)_2\cdot H_2O$ (2). L^2 (359 mg, 1.45 mmol) was dissolved in H_2O (20 mL), and the pH of the solution was adjusted to 7 with 2 M NaOH. An aqueous solution of $CuCl_2\cdot 2H_2O$ (247 mg, 1.45 mmol) in H_2O (10 mL) was added to this solution. The pH dropped to 3 and was adjusted back to 7 with 2 M NaOH. The solution was filtered and then loaded onto a Sephadex SP C25 cation-exchange column. The desired fraction eluted with a 1:1 $NaClO_4$ (0.3 M)/MeCN solution. Slow evaporation yielded the product which was then recrystallized by diffusion of Et_2O into a MeCN solution of the complex to give crystals suitable for X-ray crystallography. Yield: 0.52 g, 41%. Anal. Calcd for $C_{30}H_{54}Cl_2Cu_2N_6O_{11}$: C, 41.3; H, 6.2; N, 9.6. Found: C, 41.6; H, 6.4; N, 9.5. ESI-MS: 955.0 $[M + ClO_4]^-$. Selected IR bands (KBr disk, cm^{-1}): ν 3568s, 2865w, 1508s, 1455s, 1101vs br, 995 s, 778s, 730s, 705s, 624s. UV−vis (MeCN) λ_{max} (ϵ_{max}): 629 (103), 266 (6660), 215 nm (7280 M^{-1} cm^{-1}).

$[Cu_2(\mu_2\text{-}OH)_2L^3_2](ClO_4)_2\cdot 2H_2O$ (3). Twenty-five milligrams (53 μmol) of L^3 was mixed with 17 mg (53 μmol) of $[Cu(MeCN)_4]$-ClO_4 in 10 mL of ethanol/acetonitrile (1:1), and the mixture was allowed to stand. Green-blue crystals suitable for X-ray crystallography were obtained overnight. Yield: 20 mg, 59%. Anal. Calcd for $C_{60}H_{66}Cl_2Cu_2N_{12}O_{12}$: C, 53.6; H, 4.9; N, 12.5. Found: C, 53.5; H, 4.9; N, 12.6. ESI-MS: 1209.4 $[M - ClO_4]^+$. Selected IR bands (ATR, cm^{-1}): ν 3448b, 2232s, 1623m, 1582m, 1485m, 1441s, 1350s, 1288s, 1179w, 1158m, 1071s, 983s, 902m, 806m, 780m, 730m, 694s, 661m, 622m. UV−vis (MeCN) λ_{max} (ϵ_{max}): 891 (100), 596 (180), 281 (13 000), 273 (14 000), 227 (57 000), 205 (nm) (59 800 M^{-1} cm^{-1}).

Phosphate Ester Cleavage Kinetics. Solutions of the buffers, copper(II) complexes, and BNPP for phosphate ester cleavage studies were prepared as described previously.[1] The production of the 4-nitrophenylate ion was monitored spectrophotometrically as a function of time by monitoring the change in absorbance at 400 nm (ϵ_{max} = 18 700 M^{-1} cm^{-1}). In each experiment, a solution of the Cu(II) complex (3 mM, 1 mL) and MOPS buffer (pH 7.4, 50 °C, I = 0.382 M, 1 mL) was placed into a 1 cm cuvette which was sealed with a Teflon stopper and inverted to allow the solutions to mix. The temperature was allowed to equilibrate for 10 min; then the BNPP solution (0.045 mM, 1 mL) was added to the cuvette to give a final volume of 3.0 mL. The temperature was allowed to equilibrate again for a further 2 min, and then measurement of the absorbance change with time began. The reactions were followed for 8000 minutes with an absorbance reading taken every 5 min. The rates of BNPP hydrolysis were estimated from the plots of absorbance versus time following a procedure elaborated in the literature.[18,24] As the complex was in a large excess compared to BNPP, the appearance of NP (and cleavage of BNPP) was modeled as a first-order process. Fitting of the data to an exponential function (abs = $A + Be^{-k_{obs}t}$) gave the pseudo first-order rate constants.

X-ray Crystallography. Intensity data for a clear crystal of bis-(chloroacetamide) (0.2 × 0.2 × 0.3 mm), a dark blue crystal of **1** (0.20 × 0.12 × 0.14 mm), a dark blue crystal of **2** (0.20 × 0.15 × 0.15 mm), and a dark green crystal of **3** (0.3 × 0.25 × 0.25 mm) were measured at 123 K (230 K for **1)** on a Nonius Kappa CCD diffractometer fitted with graphite-monochromated Mo Kα radiation (0. 71073 Å). The data were collected to maximum 2θ values of 55.76, 55, 50 and 55°, respectively, and were processed using the Nonius software. Crystal parameters and details of the data

(24) Deal, K. A.; Burstyn, J. N. *Inorg. Chem.* **1996**, *35*, 2792.

Table 1. Crystallographic Data for Bis(chloroacetamide), **1**, **2**, and **3**

	bis(chloroacetamide)	**1**	**2**	**3**
empirical formula	C_4H_7ClNO	$C_{16}H_{40}Cl_2Cu_2N_6O_{10}$	$C_{30}H_{54}Cl_2Cu_2N_6O_{11}$	$C_{64}H_{68}Cl_2Cu_2N_{14}O_{10}$
M (g mol^{-1})	120.56	674.53	872.77	1391.31
cryst syst	orthorhombic	monoclinic	monoclinic	triclinic
space group	*Pbca*	$P2_1/c$	$P2_1/c$	$P\bar{1}$
a (Å)	9.975(2)	8.0961(16)	10.748(2)	17.358(4)
b (Å)	8.0632(16)	14.084(3)	16.733(3)	17.588(4)
c (Å)	13.679(3)	12.000(2)	20.725(4)	23.239(5)
α (deg)	90	90	90	75.79(3)
β (deg)	90	96.04(3)	96.39(3)	78.78(3)
γ (deg)	90	90	90	88.31(3)
V (Å^3)	1100.2(4)	1360.7(5)	3704.2(13)	6745(2)
Z	8	4	4	4
T (K)	123(2)	230(2)	123(2)	123(2)
λ (Å)	0.71073	0.71073	0.71073	0.71073
D_c (g cm^{-3})	1.456	1.954	1.565	1.371
μ(Mo Kα) (mm^{-1})	0.567	1.856	1.357	0.779
no. data measured	15798	11482	35263	98491
unique data (R_{int})	1299 (0.0865)	3083 (0.0964)	6504 (0.1160)	27 901 (0.0654)
obsd data [$I > 2(\sigma)I$]	892	2256	4680	16 781
final R1,[a] wR2[b] (obsd data)	0.0464, 0.0797	0.0477, 0.1052[a]	0.0701, 0.0906	0.0680, 0.1696
final R1, wR2 (all data)	0.0843, 0.0932	0.0761, 0.1165	0.1160, 0.1000	0.1265, 0.1993
ρ_{min}, ρ_{max} (e Å^{-3})	−0.373, 0.319	−1.054, 0.605	−0.482, 0.889	−0.797, 1.062

[a] $R = \sum(|F_o| - |F_c|)/\sum|F_o|$. [b] $wR2 = [\sum w(|F_o| - |F_c|)^2/\sum F_o^2]^{1/2}$, where $w = [\sigma^2(F_o)]^{-1}$.

collection for bis(chloroacetamide) and complexes **1**−**3** are summarized in Table 1.

Each structure was solved by direct methods and expanded using standard Fourier routines in the SHELX-97 software package.[25,26] For **1**, the hydrogens were placed in idealized positions except H(1W) and H(1N) which were located on the Fourier difference map. All the non-hydrogen atoms were refined anisotropically. In the refinement of **2**, isotropic restrictions were placed on C(13), and distance restrictions were placed on (O(1OH) H(1OH)), (O(2OH) H(2OH)), (O(1W) H(1W)), and (O(1W) H(2W)). All hydrogens, except those of H(1W)−H(4W), were placed in idealized positions. The anisotropic displacements of H(1W)−H(4W) were also restrained to be identical. All non-hydrogen atoms were refined anisotropically, except for the pyridyl C atoms C13 and C14, which were refined with isotropic thermal parameters.

For **3**, all hydrogens were placed in idealized positions except for the hydrogens on on the bridging hydroxides which were located on the Fourier difference map. One of the benzonitrile arms was disordered over two positions, and thus the occupancy of the two positions was refined. The site occupancy of the disordered water in the crystal was also modeled against its components. Because of the disordered nature of parts of the structure, isotropic restraints were placed on the anisotropic thermal parameters of a number of atoms, while the others were refined isotropically. All other non-hydrogen atoms were refined anisotropically. Because of the number of atoms in the unit cell, the anisotropic refinement was performed using a full-matrix block method.

Results and Discussion

The synthesis of the ligand L^2 (Scheme 1) was adapted from a method first described by Bradshaw et al.[27−29] This involved formation of a bis(chloroacetamide) compound, followed by cyclization with benzylamine to form diamide intermediates. The X-ray structure of the bis(chloroacetamide) (see Crystallography Section) shows that the two acyl chloride groups are well separated in the solid-state. To achieve cyclization, these two groups must rotate around the C(3)−N(1) and C(3)−C(3)′ bond so that they adopt a "cis" orientation. This rearrangement may be unfavorable and may represent an appreciable energy barrier to cyclization that affects the yield of the diamide. Slow addition of the benzylamine to the reaction mixture was found to promote cyclization over the formation of oligomeric species. Reduction of the diamides was achieved using $LiAlH_4$ to afford L^2. The synthesis of L^2 was confirmed by ESI-MS, which showed a peak at 248.3 *m*/*z* corresponding to the molecular ion $[M + H]^+$, and by ^1H and ^{13}C NMR spectroscopy. Ligand L^3 was synthesized in one step by reaction of the hydrochloride salt of tacn with 3-cyanobenzylbromide in aqueous solution (Scheme 2). The neutral ligand that was extracted from the reaction mixture was spectroscopically pure and was used without further purification.

Scheme 1. Synthesis of L^2

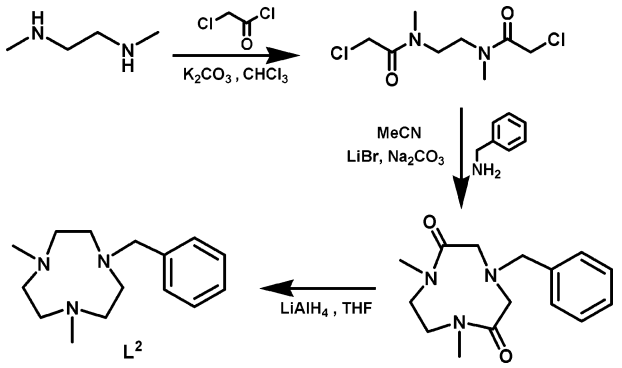

The copper(II) complex of L^1, $[Cu_2(\mu_2-OH)_2L^1_2](ClO_4)_2$ (**1**), was crystallized from an aqueous solution of $CuCl_2 \cdot 2H_2O$ and L^1 adjusted to a pH of 9, following the addition

(25) Sheldrick, G. M. *SHELXL-97*; University of Göttingen: Göttingen, Germany, 1997.
(26) Sheldrick, G. M. *SHELXS-97*; University of Göttingen: Göttingen, Germany, 1997.
(27) Bradshaw, J. S.; Krakowiak, K. E.; Izatt, R. M. *Tetrahedron Lett.* **1989**, *30*, 803.
(28) Krakowiak, K. E.; Bradshaw, J. S.; Izatt, R. M. *J. Heterocycl. Chem.* **1989**, *26*, 1431.
(29) Krakowiak, K. E.; Bradshaw, J. S.; Izatt, R. M. *J. Org. Chem.* **1990**, *55*, 3364.

Scheme 2. Synthesis of L^3

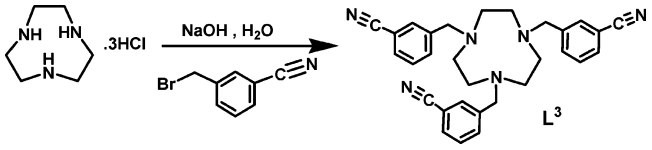

of $NaClO_4$. The copper complex of L^2, $[Cu_2(\mu\text{-}OH)_2L^2_2](ClO_4)_2 \cdot H_2O$ (**2**),was formed in a similar manner; however the workup involved additional purification by cation-exchange chromatography. Elemental analysis confirmed the proposed composition of the complexes.

The complex of L^3, $[Cu_2(\mu\text{-}OH)_2L^3_2](ClO_4)_2 \cdot H_2O$ (**3**), was formed via the reaction of $[Cu(CH_3CN)_4](ClO_4)$ with an acetonitrile/ethanol solution of the free ligand, followed by slow air oxidation. This yielded crystals of **3** suitable for X-ray analysis. The bridging hydroxo groups originate from the reduction of dioxygen by the Cu(I) (itself oxidized to Cu(II)), traces of water in the solvents, or both. There are literature precedents reporting that air oxidation of Cu(I)−tacn complexes results in hydroxo-bridged complexes. Tolman et al showed that Cu(I) bound by tacn derivatives would bind oxygen as a superoxide ion at −80 °C and, at the same time, one Cu(I) center would be oxidized; when the mixture was warmed to room temperature, further oxidation of copper was found occur, which was accompanied by the reduction of superoxide and hydroxide-bridge formation.[30] A discussion of this mechanism can be found in the literature.[31,32]

The UV−vis spectra of complexes **1**, **2**, and **3** show a d → d transition at 624 (ϵ = 86 M^{-1} cm^{-1}), 629 (ϵ = 103 M^{-1} cm^{-1}), and 596 nm (ϵ = 180 $M^{-1}cm^{-1}$), respectively, which are in the typical wavelength range for Cu(II)−tacn complexes with distorted octahedral or square pyramidal geometries.[33] Complex **1** exhibited a MLCT transition at 260 nm (ϵ = 5260 M^{-1} cm^{-1}), while for **2**, $\pi \rightarrow \pi^*$ ligand or charge-transfer transitions were found at 266 (ϵ = 6660 M^{-1} cm^{-1}) and 215 nm (ϵ = 7280 M^{-1} cm^{-1}). For **3**, intense $\pi \rightarrow \pi^*$ or charge-transfer transitions were observed at 281 (ϵ = 13 000 M^{-1} cm^{-1}), 273 (ϵ = 14 000 M^{-1} cm^{-1}), 227 (ϵ = 57 000 M^{-1} cm^{-1}), and 205 nm (ϵ = 59 800 M^{-1} cm^{-1}).

Crystal Structure Determinations. Bis(chloroacetamide). The X-ray structure analysis of this compound (Figure 1) revealed the extended nature of the molecule in the crystalline state, highlighted by the trans orientation of the methyl and amide substituents. The bond lengths of C(2)−N(1) and C(2)−O(1) reveal that they both exhibit partial double-bond character, as is typical for amide bonds, which suggests that rotation through the C(2)−N(1) bond may be restricted. This feature may have affected the cyclization reaction between the bis(chloroacetamide) and the benzylamine compounds (vide supra). **Complex 1.** A single-crystal X-ray structure determination of **1**, performed at 230 K to avoid the cracking of the crystal observed at 193 K, confirmed the binuclear nature of the complex cation (see Figure 2). The structure reveals the formation of a μ_2-hydroxo-bridged dicopper(II) core, with each end capped by a facially coordinating Me_2tacn (L^1) ligand. Only half of the dimer resides in the asymmetric unit (ASU), with the other half generated by symmetry, so that the two copper centers are crystallographically equivalent. The copper centers are in a distorted square pyramidal geometry with similar bond angles and distances (Table 3). Using the Addison et al.[34] measure for the degree of deviation from square pyramidal geometry toward trigonal bipyramidal geometry, this system gives τ = 1.7% (τ = [{($\theta - \varphi$)/60}100], where θ and φ are

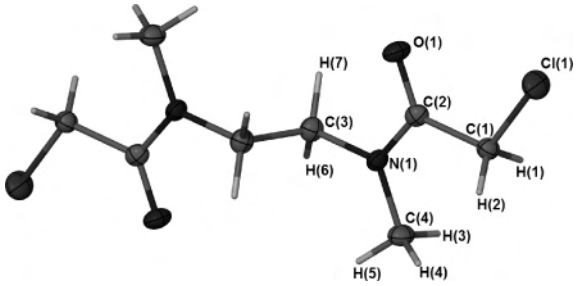

Figure 1. ORTEP representation of the bis(chloroacetamide) compound (thermal ellipsoids drawn at 50% probability).

Table 2. Selected Bond Lengths (Å) and Angles (deg) in the Bis(chloroacetamide)[a]

Cl(1)−C(1)	1.778(2)	C(2)−N(1)−C(4)	123.26(18)
O(1)−C(2)	1.229(3)	C(2)−N(1)−C(3)	118.41(17)
N(1)−C(2)	1.347(3)	C(4)−N(1)−C(3)	118.00(17)
N(1)−C(4)	1.459(3)	C(2)−C(1)−Cl(1)	111.40(16)
N(1)−C(3)	1.467(3)	O(1)−C(2)−N(1)	122.4(2)
C(1)−C(2)	1.510(3)	O(1)−C(2)−C(1)	122.47(19)
C(3)−C(3)#1	1.523(4)		

[a] esd in parentheses.

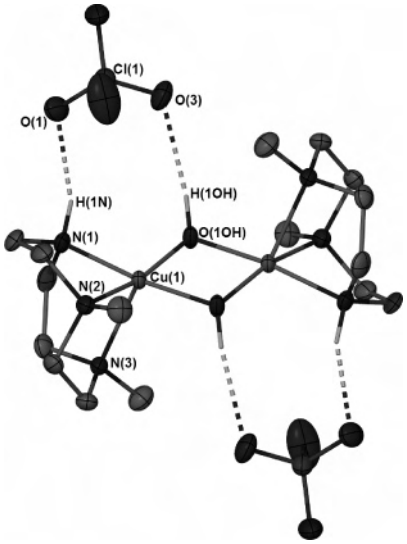

Figure 2. ORTEP representation of the binuclear complex of **1** (thermal ellipsoids drawn at 50% probability and certain hydrogens omitted for clarity; dashed bonds indicated H-bonds).

(30) Mahapatra, S.; Halfen, J. A.; Wilkinson, E. C.; Pan, G.; Wang, X.; Young, V. G.; Cramer, C. J.; Que, L.; Tolman, W. B. *J. Am. Chem. Soc.* **1996**, *118*, 11555.
(31) Mahapatra, S.; Halfen, J. A.; Tolman, W. B. *J. Am. Chem. Soc.* **1996**, *118*, 763.
(32) Mahapatra, S.; Halfen, J. A.; Tolman, W. B. *J. Am. Chem. Soc.* **1996**, *118*, 11575.
(33) Cotton, F. A.; Wilkinson, G.; Murillo, C. A.; Bochmann, M. *Advanced Inorganic Chemistry*, 6th ed.; Wiley-Interscience: New York, 1999.
(34) Addison, A. W.; Rao, T. N.; Reedijk, J.; van Rijn, J.; Verschoor, G. C. *J. Chem. Soc., Dalton Trans.* **1984**, 1349.

Table 3. Selected Bond Lengths (Å) and Angles (deg) in **1**[a]

O(1OH)−Cu(1)−O(1OH)[b]	82.09(12)	Cu(1)−Cu(1)[b]	2.9359(12)
N(1)−Cu(1)−N(2)	84.43(13)	Cu(1)−N(1)	2.011(3)
N(1)−Cu(1)−N(3)	82.46(11)	Cu(1)−N(2)	2.093(3)
N(2)−Cu(1)−N(3)	82.56(11)	Cu(1)−N(3)	2.256(3)
Cu(1)−O(1OH)−Cu(1)[b]	97.91(12)	Cu(1)−O(1OH)	1.941(3)
		Cu(1)−O(1OH)[b]	1.952(3)

[a] esd in parentheses. [b] Symmetry transformations used to generate equivalent atoms: $-x, -y, -z$.

Table 4. Selected Bond Lengths (Å) and Angles (deg) in **2**[a]

Cu(1)−Cu(2)	2.889(12)	N(1)−Cu(1)−N(2)	82.46(14)
Cu(1)−N(1)	2.285(4)	N(2)−Cu(1)−N(3)	84.81(14)
Cu(1)−N(2)	2.073(4)	N(3)−Cu(1)−N(1)	82.36(13)
Cu(1)−N(3)	2.064(4)	N(4)−Cu(2)−N(5)	84.69(14)
Cu(2)−N(4)	2.085(4)	N(5)−Cu(2)−N(6)	83.36(14)
Cu(2)−N(5)	2.073(4)	N(6)−Cu(2)−N(4)	83.06(14)
Cu(2)−N(6)	2.260(4)	O(1OH)−Cu(1)−O(2OH)	82.07(13)
Cu(1)−O(1OH)	1.926(3)	O(1OH)−Cu(2)−O(2OH)	82.00(14)
Cu(1)−O(2OH)	1.944(3)	Cu(1)−O(1OH)−Cu(2)	97.04(14)
Cu(2)−O(1OH)	1.930(3)	Cu(1)−O(2OH)−Cu(2)	96.04(14)
Cu(2)−O(2OH)	1.942(3)		

[a] esd in parentheses.

the largest and second-largest angles in the basal plane. The small τ value indicates that the geometry is close to square pyramidal (as shown in Figure 2). The two axial nitrogens are trans to each other, and the axial Cu−N distance is elongated by >0.15 Å with respect to those in the Cu−N basal plane.

The perchlorate anion H-bonds to the secondary amine hydrogen from the L^1 macrocycle and the hydrogen from the bridging hydroxyl group with H−O distances of 2.080(4) and 2.279(5) Å, respectively. Other than these H-bonds, which cannot form in the Me_3tacn complex because there is no secondary amine to act as a H-bond donor, the structure is broadly similar to that of $[Cu_2(\mu_2\text{-}OH)_2(Me_3tacn)_2]^{2+}$.[10] As in $[Cu_2(\mu_2\text{-}OH)_2(Me_3tacn)_2]^{2+}$, the hydrogen atoms on the bridging hydroxides are located in a trans arrangement with respect to the plane of the $[Cu(\mu_2\text{-}OH)_2]^{2+}$ bridge. This is illustrated in Figure 9, which shows the two general geometries that the dihydroxo core has been found to adopt in tacn-based copper(II) dimers. There are some subtle structural differences in the $[Cu_2(\mu_2\text{-}OH)_2]$ core for the two complexes. While the Cu−O distances are similar, 1.94−1.95 Å, the Cu···Cu separation is shorter in the Me_2tacn complex because of the the more acute Cu−O−Cu angles (viz, 97.9 ° vs 100.1 °).

Complex 2. The X-ray structure of **2** reveals a dicopper core, consisting of two Cu(II) centers bridged by two hydroxo ligands and capped by a facially coordinating L^2 ligand. The two metal centers are not related by symmetry and are crystallographically inequivalent. However, both are five coordinate and have distorted square pyramidal geometry (τ = 4.1%). All N−Cu−N angles are below 90° (Table 4) because of the constraints that the tridentate tacn macrocycle places on the geometry. The O−Cu−O angles are also below 90°, and these constraints result in N−Cu−O angles that are greater than 90°. The Cu−O−Cu bridge angles are nearly identical (97.04(1) and 96.04(1)° for O(1OH) and O(2OH), respectively), and they are similar to the corresponding angles in **1**. An interesting feature of the complex is that the O(1OH) hydroxide bridge participates in H-bonding with the water molecule in the lattice (see Figure 3). The effects of this H-bond are exhibited in a slight difference of 1° in the Cu(1)−O(1OH)−Cu(2) angle compared to the non-H-bonded Cu(1)−O(2OH)−Cu(2) angle. There are also subtle differences in the Cu−O distances, both those involving O(1OH) being shorter than the Cu−O(2OH) distances.

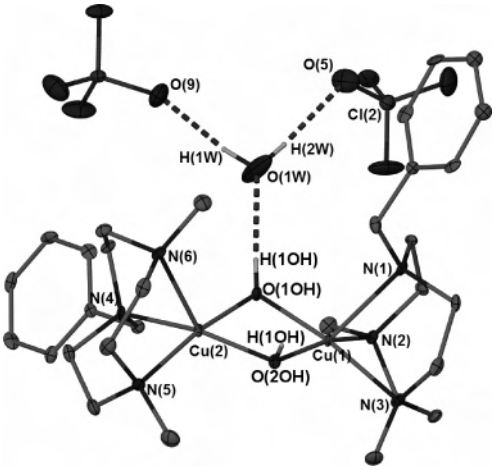

Figure 3. ORTEP representation of complex **2** showing H-bonding as dashed bonds (thermal ellipsoids drawn at 50% probability and hydrogen atoms omitted for clarity).

The copper−dihydroxo core in this complex is markedly different from that found in **1** and $[Cu_2(\mu_2\text{-}OH)_2(Me_3tacn)_2]^{2+}$.[10] In **2**, the core adopts a bent, roof-shaped configuration (see Figure 9), and the hydrogens of the hydroxide groups, which were clearly recognizable in the Fourier difference map, are cis with respect to the $[Cu_2(\mu_2\text{-}O)_2]$ core rather than in the trans orientation adopted by the other two compounds. A least-squares plane analysis of the core reveals that the dihedral angle (δ) across the core is 162.8°. This results in a shorter Cu···Cu distance (2.889(12) Å) than those in the Me_3tacn complex and **1**, which have a Cu···Cu distances of 2.971(1) and 2.939(11) Å, respectively.[10]

Complex 3. The X-ray crystal structure of **3** established the presence of two nonsymmetry-related hydroxo-bridged copper dimers (one of which is illustrated in Figure 4). Again there is elongation of the apical position of the square pyramid by 0.15 Å with respect to the basal coordination sites. Of the three new complexes reported herein, complex **3** has the largest deviation from square pyramidal, with $\tau_{Cation1}$ = 17% and $\tau_{Cation2}$ = 15%. One of the complex cations shows a slight 0.2° difference in the two Cu−O−Cu angles, generating some asymmetry in the $[Cu_2(\mu_2\text{-}OH)_2]^{2+}$ core. The second complex cation in the asymmetric unit has a more symmetrical core, with the Cu−O−Cu angles being 94.16(13) and 94.08(13)°.

As is **2**, the $[Cu_2(\mu_2\text{-}OH)_2]^{2+}$ cores of both cationic units adopt the roof-shaped configuration, with the hydroxyl hydrogen atoms clearly located on the Fourier difference map. The dihedral angles for the two complex cations in the asymmetric unit are 160.38(12) and 151.61(19)°. The former is quite similar to that observed in **2**. For each cation, the pendant cyanobenzyl groups from the two capping

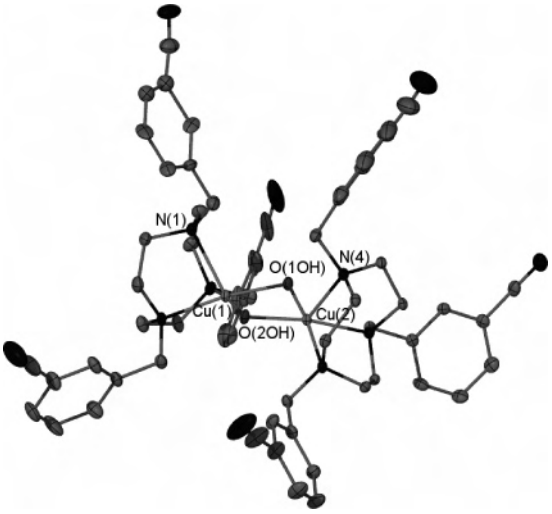

Figure 4. ORTEP representation of the complex cation in **3** (thermal ellipsoids drawn at 50% probability, and hydrogen atoms, solvent, and counterions omitted for clarity).

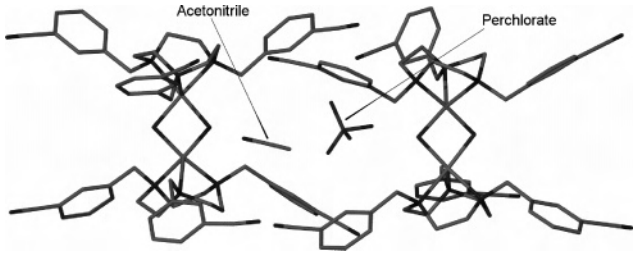

Figure 5. Hydrophobic pocket in the packing of **3** (hydrogen atoms, selected counterions, and other solvent molecules omitted for clarity).

ligands are all eclipsed with respect to each other when viewed down the Cu···Cu axis in one binuclear cation. The same is true for four of the six groups in the other cation. This feature contributes to the lower symmetry in the crystal system.

Interestingly, there is no hydrogen bonding in the crystal lattice of **3**, most probably because of the steric hindrance of the bulky cyanobenzyl pendant arms on the macrocycle. A notable feature of the crystal packing is that a perchlorate anion and a molecule of acetonitrile are encapsulated in the hydrophobic pockets that are generated by the bulky cyanobenzyl groups (see Figure 5).

A comparison of the structural features of the $[Cu_2(\mu\text{-}OH)_2]^{2+}$ core in complexes **1**−**3** with those of other copper complexes is given in Table 6. One notable observation is that the $[Cu_2(\mu\text{-}OH)_2]^{2+}$ cores in known complexes of monomacrocyclic tacn ligands and **1** are planar and symmetric, with the hydroxide hydrogens adopting a trans configuration with respect to the $[Cu_2(\mu\text{-}O)_2]$ unit. In contrast, the $[Cu_2(\mu\text{-}OH)_2]^{2+}$ cores in **2** and **3** adopt a roof-shaped geometry in which the hydroxo hydrogens are cis relative to the $[Cu_2(\mu\text{-}OH)_2]$ unit. Previously, such a structural feature has only been identified in complexes of bis-, tris-, and tetrakis-tacn ligands in which the macrocyclic compartments are linked via the meta positions in aromatic tethers, such as *m*-xylylene, mesitylene, and durene.[11−13] In complexes **2** and **3**, this feature gives rise to very interesting magnetic properties (vide infra). A further consequence of the roof-shaped geometry is that the Cu···Cu separation is quite short in complexes **2** and **3**, again more typical of hydroxo-bridged complexes in which the roof-shaped geometries are supported by aromatic spacers (see Table 6). The effect of the dihedral angle (δ) on the Cu···Cu separation is clearly highlighted by $[Cu_2(CH_3NH_2)_4(\mu\text{-}OH)_2](SO_4)\cdot H_2O$.[35] In this complex, the short Cu−Cu separation of 2.782(5) Å can be attributed to the very tight dihedral angle of 133°. In keeping with this, in **2** and **3**, dihedral angles of 160−163° result in a Cu···Cu distance of 2.89 Å, while a dihedral angle of 152° gives a separation of 2.84 Å. Similar general trends are evident in hydroxo-bridged copper(II) complexes of multi-tacn ligands, although other subtleties are evident in those systems (see Table 6).[10−13,30,35−39]

Table 5. Selected Bond Lengths (Å) and Angles (deg) in **3**[a]

Cu(1)−Cu(2)	2.8879(13)	Cu(1)−O(1OH)−Cu(2)	95.78(13)
Cu(1)−O(1OH)	1.944(3)	Cu(2)−O(2OH)−Cu(1)	96.03(13)
Cu(1)−O(2OH)	1.945(3)	Cu(4)−O(3OH)−Cu(3)	94.16(13)
Cu(2)−O(2OH)	1.940(3)	Cu(4)−O(4OH)−Cu(3)	94.08(13)
Cu(2)−O(1OH)	1.949(3)	N(2)−Cu(1)−N(1)	82.73(14)
Cu(1)−N(2)	2.079(4)	N(3)−Cu(1)−N(1)	82.67(13)
Cu(1)−N(3)	2.088(3)	N(2)−Cu(1)−N(3)	84.85(14)
Cu(1)−N(1)	2.283(4)	N(6)−Cu(2)−N(5)	85.21(14)
Cu(2)−N(6)	2.079(4)	N(6)−Cu(2)−N(4)	83.50(13)
Cu(2)−N(5)	2.100(3)	N(5)−Cu(2)−N(4)	83.02(13)
Cu(2)−N(4)	2.250(4)	N(14)−Cu(3)−N(13)	85.40(14)
Cu(3)−Cu(4)	2.8426(13)	N(14)−Cu(3)−N(15)	83.58(14)
Cu(3)−O(4OH)	1.942(3)	N(13)−Cu(3)−N(15)	84.65(13)
Cu(3)−O(3OH)	1.944(3)	N(19)−Cu(4)−N(21)	85.12(14)
Cu(4)−O(3OH)	1.938(3)	N(19)−Cu(4)−N(20)	83.80(10)
Cu(4)−O(4OH)	1.942(3)	N(21)−Cu(4)−N(20)	84.02(11)
Cu(3)−N(14)	2.060(4)		
Cu(3)−N(13)	2.064(3)		
Cu(3)−N(15)	2.278(4)		
Cu(4)−N(19)	2.073(3)		
Cu(4)−N(21)	2.077(4)		
Cu(4)−N(20)	2.245(4)		

[a] esd in parentheses.

Magnetism. Hydroxo bridges between Cu(II) centers, such as those found in complexes **1**−**3** are known to mediate magnetic interactions between the metal centers, and with one exception, these interactions have invariably been antiferromagnetic in nature (see Table 6). With this in mind, variable-temperature magnetic susceptibility measurements were performed on powder samples of **1**−**3** to examine the nature of such interactions in these complexes. The measurements were carried out in the 4.2−300 K temperature range in a field of 1 T. Plots of magnetic moment versus temperature for **1**−**3** for can be seen in Figures 6−8.

Figure 6 shows that the magnetic moment decreases from a value of 1.62 μ_B (per Cu) at 300 K to 0.54 μ_B at 4.2 K. The corresponding χ_{Cu} versus T plot shows a maximum at 50 K and a rapid rise at low temperature resulting from monomer impurity. This indicates that antiferromagnetic

(35) Charlot, M. F.; Jeannin, S.; Jeannin, Y.; Kahn, O. *Inorg. Chem.* **1980**, *19*, 1410.
(36) Farrugia, L. J.; Lovatt, P. A.; Peacock, R. D. *Inorg. Chim. Acta* **1996**, *246*, 343.
(37) Evans, A. J.; Watkins, S. E.; Craig, D. C.; Colbran, S. B. *J. Chem. Soc., Dalton Trans.* **2002**, 983.
(38) Rojas, D.; Garcia, A. M.; Vega, A.; Moreno, Y.; Venegas-Yazigi, D.; Garland, M. T.; Manzur, J. *Inorg. Chem.* **2004**, *43*, 6324.
(39) Chou, C.-C.; Su, C.-C.; Tsai, H.-L.; Lii, K.-H. *Inorg. Chem.* **2005**, *44*, 628.

Table 6. Structural and Magnetic Data for a Selection of Cu(II) Complexes with $[Cu_2(\mu\text{-}OH)_2]$ Cores

complex	Cu−O (Å)	Cu−Cu′ (Å)	Cu−O−Cu′ (deg)	δ (deg)	J (cm^{-1})	ref
1	1.941(3)	2.9359(12)	97.91(12)	180	−36.4	this work
	1.952(3)		97.91(12)			
2	1.926(3)	2.889(12)	97.04(14)	162.8	11.2	this work
	1.944(3)		96.04(14)			
3 (Cation1, [Cation2])	1.944(3),	2.8879(13),	95.78(13),	160.38(12),	49.3	this work
	[1.942(3)]	[2.8426(13)]	[95.78(13)]	[151.61(19)]		
	1.945(3),		96.03(13),			
	[1.944(3)]		[96.03(13)]			
$[Cu_2(Me_3tacn)_2(\mu\text{-}OH)_2](ClO_4)_2$[a]	1.939(4)	2.971(1)	100.1(2)	180	−45	10
	1.936(4)		100.1(2)			
$[Cu_2(Me_3tacn)_2(\mu\text{-}O)(\mu\text{-}OH_2)](ClO_4)_2$	2.220(5)	3.03(1)	88.6(2)		37	10
$[Cu_2L^{mx}(\mu\text{-}OH)_2](BPh_4)_2$[b]	1.928(2)	2.9464(5)	99.55(10)	173.5	−159	11
	1.931(2)		99.56(10)			
$[Cu_4L^{dur}(\mu\text{-}OH)_4](ClO_4)_4$[c]	1.961(8)	2.939(9)	97.9(4)	158	−27	12
	1.975(8)		95.7(4)			
$[Cu_3L^{mes}(\mu\text{-}OH)_2](ClO_4)_4$[d]	1.900(5)	2.9041(8)	98.9(2)	152	−24	13
	2.019(3)		92.1(1)			
$[Cu_3L^{mes}(\mu\text{-}OH)_2]_2(\mu\text{-}OH)_2(ClO_4)_6$,[d] bent	1.920(3)	2.8757(8)	94.7(1)	153	−61	13
	1.957(3)		97.0(1)			
$[Cu_3L^{mes}(\mu\text{-}OH)_2]_2(\mu\text{-}OH)_2(ClO_4)_6$,[d] planar	1.933(4)	2.961(1)	98.7(2)	180	−29	13
	1.969(4)					
$[Cu_2(Butacn)_2(\mu\text{-}OH)_2](ClO_4)_2$[e]	1.929(2)	2.9778(8)	101.01(9)	180	NR	36
$[Cu_2(Fc^iPr_2tacn)_2(\mu\text{-}OH)_2](ClO_4)_2$[f]	1.960(7)	3.017(3)	101.1(3)	180	NR	37
	1.946(7)					
$[(L^{Bn3}Cu)(L^{Bn2H}Cu)(\mu\text{-}OH)_2](CF_3SO_3)_22(^iPrOH)$[g]	1.949(4)	2.9769(9)	100.5(2)	169.4	NR	30
	1.924(5)		100.8(2)			
[(L^{i}Pr2HCu)2(μ-OH)2](BPh4)2.2THF[h]	1.922(6)	3.0088(13)	100.9(3)	178.5	NR	30
	1.951(6)		102.7(3)			
[(L^{i}Pr2BnCu)2(μ-OH)2](CF3SO3)2[i]	1.950(6)	3.037(3)	101.1(3)	180	NR	30
	1.933(6)		102.9(3)			
$[Cu_2(C_6H_{11}NH_2)_4(\mu\text{-}OH)_2](ClO_4)_2$	1.960(5)	2.934(8)	96.6(2)	148	−128	7
	1.923(5)		99.7(2)			
$[Cu_2(CH_3NH_2)_4(\mu\text{-}OH)_2](SO_4).H_2O$	1.99(1)	2.782(5)	91.7(7)	133	−4	35
	1.94(1)		88.6(7)			
$[Cu(FDPMA)(\mu\text{-}OH)_2]_2(ClO_4)_2$[j]	1.923(5)	2.960(1)	100.3(2)	180	−97.5	38
	1.931(5)		100.7(2)			
$[Cu_2(H_2CPz_2)_2(\mu\text{-}OH)_2(ClO_4)](ClO_4)$[k]	1.920(2)	2.873(3)	96.6(1)	153.1	Θ = 4.4 K	39
	1.949(2)		94.9(1)			

[a] Me_3tacn = 1,4,7-trimethyl-1,4,7-triazacyclononane. [b] L^{mx} = 1,3-bis(1,4,7-triazacyclonon-1-ylmethyl)benzene. [c] L^{dur} = 1,2,4,5-tetrakis(1,4,7-triazacyclonon-1-ylmethyl)benzene. [d] L^{mes} = 1,3,5-tris(1,4,7-triazacyclonon-1-ylmethyl)benzene. [e] Butacn = *N*-4-but-1-ene-1,4,7-triazacyclononane. [f] 1-Ferrocenylmethyl-4,7-diisopropyl-1,4,7-triazacyclononane. [g] L^{Bn3} = 1,4,7-tribenzyl-1,4,7-triazacyclononane; L^{Bn2H} = 1,4-dibenzyl-1,4,7-triazacyclononane. [h] L^{i}Pr2H = 1,4-diisopropyl-1,4,7-triazacyclononane. [i] L^{i}Pr2Bn = 1-benzyl-4,7-diisopropyl-1,4,7-triazacyclononane. [j] FDPMA = (2-pyridylmethyl)(6-trifluoromethyl-2-pyridylmethyl)-benzylamine. [k] H_2CPz_2 = bis(pyrazol-1-yl)-methane). [l] NR = not reported.

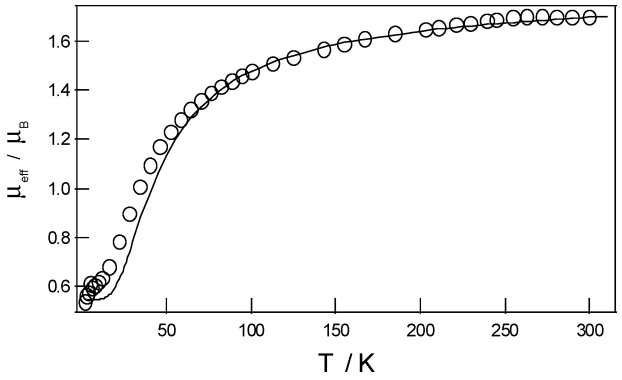

Figure 6. Plot of μ_{eff} (per Cu) vs temperature for **1**. The solid line is the best-fit obtained using $g = 1.99 \pm 0.01$, $N_\alpha = (60 \pm 5) \times 10^{-6}$ cm^3 mol^{-1}, $J = -36.4 \pm 0.2$ cm^{-1}, and $x = 0.1 \pm 0.01$ (monomer impurity).

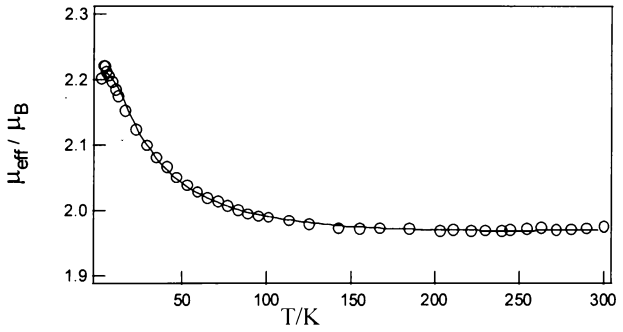

Figure 7. Plot of μ_{eff} (per Cu) vs temperature for **2**. The solid line is the best fit obtained using g = 2.2 ± 0.01, $N_\alpha = (60 \pm 5) \times 10^{-6}$ cm^3 mol^{-1}, and $J = 11.2 \pm 0.2$ cm^{-1}.

coupling is occurring. The data were modeled using a $-2JS_1S_2$ Bleaney−Bowers approach,[40] and the best-fit parameters are $g = 1.99 \pm 0.01$, $J = -36.4 \pm 0.2$ cm^{-1}, $N_\alpha = (60 \pm 5) \times 10^{-6}$ cm^3 mol^{-1} (temperature-independent paramagnetic susceptibility), and $x = 0.1 \pm 0.01$ (monomer fraction).

The fit is good above 70 K but fair below this because of the effect the monomer impurity has on the least-squares fitting. The best-fit g value is also a bit lower than the normal value of ∼2.1. The J value calculated from the position of the maximum in the χ_{Cu} plot is -28 cm^{-1}, suggesting that the value obtained from the best fit over the range of 4.2−300 K is influenced by the higher than normal fraction of monomer impurity. Nevertheless, the excellent microanalysis

(40) Bleaney, B.; Bowers, K. D. *Proc. R. Soc. London, Ser. A* **1952**, *214*, 541.

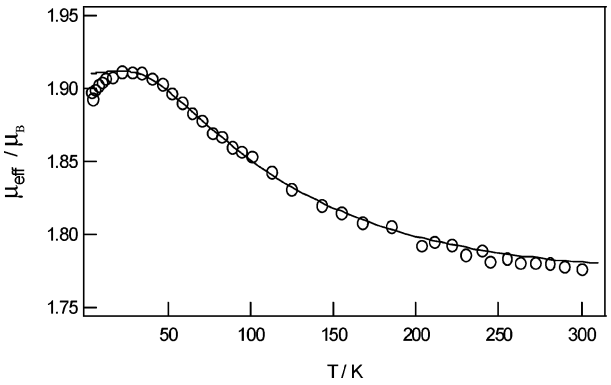

Figure 8. Plot of μ_{eff} (per Cu) vs temperature for **3**. The solid line is the best fit obtained using $g = 1.91 \pm 0.01$, $N_\alpha = (65 \pm 5) \times 10^{-6}$ cm^3 mol^{-1}, and $J = 49.3 \pm 0.2$ cm^{-1}.

on this highly crystalline compound leaves us in no doubt as to the integrity of the material.

The plot of magnetic moment versus temperature for **2** (Figure 7) shows that the magnetic moment increases from a value of 1.85 μ_B (per Cu) at 300 K to a value of 2.20 μ_B at 4.2 K. This indicates that ferromagnetic coupling is occurring to yield a $S = 1$ ground state. Such a ferromagnetic interaction is unusual for di-μ_2-hydroxo-bridged dicopper complexes of tacn-based ligands,[12] but it has been observed for other (LCu(μ-OH)$_2$CuL) compounds.[6] The best-fit parameters for **2** are $g = 2.2 \pm 0.01$, $N_\alpha = (60 \pm 5) \times 10^{-6}$ cm^3 mol^{-1}, and $J = 11.2 \pm 0.2$ cm^{-1}.

Figure 8 shows the plot of magnetic moment versus temperature for **3**. It clearly shows a ferromagnetic interaction, with the magnetic moment increasing from 1.78 μ_B (per Cu) at 300 K to 1.91 μ_B at 30 K, followed by a small decrease to 1.89 μ_B at 4.2 K. Fitting of the data gives $J = 49.3 \pm 0.2$ cm^{-1}. The low value of g in this case is related to the ready loss of hydrated water that influences the sample and molar mass.

Crawford et al. have derived an empirical formula for copper dimers that relates structural parameters to the observed value of the exchange constant (J).[6] It was found that the J shows a linear correlation with the Cu−O−Cu angle (ϕ) for complexes with planar or near-planar Cu$_2$(μ_2-OH)$_2$ cores, according to the equation $2J = -74.53\phi + 7270$ cm^{-1}. The crossover from ferromagnetic to antiferromagnetic coupling is at $\phi = 97.5°$, a value close to those observed here (see Table 6). According to this equation, complex **1** should have a value of $J = -13.6$ cm^{-1}, which is higher (more positive) than the observed value of $J = -36.4$ cm^{-1}. Similarly for **2**, the equation predicts a J value of 37.3 cm^{-1}, which is higher than the observed value of 11.2 cm^{-1}, but it is consistent with the ferromagnetic coupling observed. For **3**, the calculated J value of 33 cm^{-1} being much closer to the fitted value.

It is tempting to try and correlate the different J values noted in complexes **1**−**3**, as well as the discrepancies between the fitted values and those calculated from the Crawford et al. equation, in terms of other factors known to influence the J values in dihydroxo-bridged Cu(II) compounds. Such factors include the dihedral angle (δ)[7,35] in roof-shaped dimers such as **2** and **3** (see Figure 9) and the out-of-Cu$_2$O$_2$ plane displacement of the hydroxo H atom,[9] the latter emanating from DFT calculations of singlet−triplet energy levels. The trends are correct, but the small range of J values, as well as the effects upon J of the hydrogen bonding to the OH group by anion in **1** and solvated water in **2**, make such correlations of limited value.

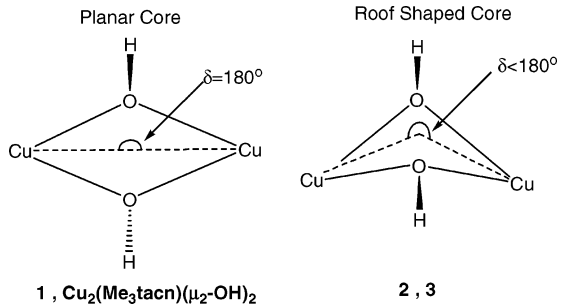

Figure 9. Comparison of the [Cu$_2$(μ_2-OH)$_2$] core geometry of **1**−**3** and the reported complex [Cu$_2$(Me$_3$tacn)$_2$(μ_2-OH)$_2$]$^{2+}$.[10]

It is interesting to speculate on the nature of the proposed μ-oxo-μ-aqua bridged Me$_3$tacn dimer,[10] the fine structural details of which could not be refined because of the disorder at the bridging oxygen. The J value suggests that this material might be like **2** and **3**, having a roof shaped geometry and perhaps involving aquo−hydroxo H-bonds. The color and λ_{max} values for this complex are also similar to those of **2** and **3**. However, the Cu···Cu separation and Cu−O−Cu angles do not follow the trends in Table 5.

Phosphate Ester Cleavage Screening Studies. The ability of complexes **1**−**3** to cleave phosphate esters was explored through a study of their rate of cleavage of the model phosphodiester, bis(*p*-nitrophenyl)phosphate), BNPP. Cleavage of BNPP releases the *p*-nitrophenylate ion (NP), a chromophore which absorbs strongly at 400 nm. The reaction of BNPP with the Cu(II) complexes was followed by UV−vis spectrophotometry under the same conditions ([complex] = 1.0 mM, [BNPP] = 0.15 mM, pH = 7.4 (MOPS), T = 50 °C, [ionic strength] = 0.15 M (NaClO$_4$)). Because of the poor solubility of **2** and **3** in H$_2$O the reactions were followed in a 1:3 MeCN/H$_2$O mixture. The previously studied [Cu(Me$_3$tacn)(OH$_2$)]$^{2+}$ system was examined under the same conditions so that a meaningful comparison of reactivity could be made.[1−5]

The copper(II) complexes reported herein were all found to effectively hydrolyze BNPP, the observed rates being within 5-fold of the rates reported for the very effective Cu(II)−Me$_3$tacn and Cu(II)−^{i}Pr$_3$tacn complexes. The data further confirms that alkylation of the secondary nitrogens on the tacn macrocycle results in significant increases in reactivity. Indeed the data in Table 6 indicate that methylation of two of the three secondary nitrogens results in a 40-fold increase in hydrolysis rate (cf. 100 for the Me$_3$tacn complex). The data (Table 7) also indicate significant variations in reactivity. In particular, of all the Cu−tacn derivatives studied so far, **3** exhibits the fastest rate of BNPP hydrolysis, the rate being 3-fold faster than that observed for the Cu(II)−Me$_3$tacn complex under the same conditions. On the other hand, **2** shows similar reactivity to the Me$_3$tacn complex, while a slower reaction rate was found for **1**. In general terms,

Table 7. Comparison of Rates of Cleavage of BNPP by Copper(II)−tacn Complexes[a]

compound	k ($\times 10^5$ s^{-1})	ref
OH^- at 100 °C	0.04	1
Cu(II)−tacn	0.34	1
Cu(II)−^{i}Pr$_3$tacn	4.3	1
Cu(II)−Me$_3$tacn	3.7	1
Cu(II)−Me$_3$tacn[b]	11.2 ± 0.3	this work
1	1.24 ± 0.02	this work
2[b]	7.01 ± 0.02	this work
3[b]	30.2 ± 0.2	this work

[a] Conditions used were as follows: [BNPP] = 0.015 mM, [complex] = 1.0 mM, I = 0.15 M ($NaClO_4$), T = 50 °C, pH = 7.4 (buffered with MOPS). [b] Solvent mixture of 1:3 MeCN/H_2O used to improve solubility.

the order of reactivity tacn ≪ Me$_2$tacn (L^1) < Me$_2$Bztacn (L^2) ≈ ^{i}Pr$_3$tacn ≈ Me$_3$tacn < NCBz$_3$tacn (L^3) reflects the steric bulk of the ligands when attached to Cu(II) centers. In rationalizing this observation, it should be recognized that the generally accepted mechanism for BNPP cleavage by Cu−tacn complexes involves coordination of BNPP followed by intramolecular attack by a copper-bound hydroxo group (Scheme 3) and that dimerization of the deprotonated complex, $[(tacn)Cu(OH)OH_2]^+$, produces the hydrolytically inactive $[(tacn)Cu(OH)_2Cu(tacn)]^{2+}$ complex. The observed reactivity changes are subtle but may result from changes in the acidity of coordinated water molecules and a decreased tendency for the deprotonated complex to dimerize for complexes of the bulkiest tacn derivative, L^3. On the other hand, the L^2 complex behaves in a manner similar to that of the Me$_3$tacn complex since, in forming the hydroxo bridged dimer, the benzyl groups can be well separated, minimizing the steric barrier to dimer formation, although it should be noted that this compound does adopt a roof-shaped dihydroxo-bridged core.

Conclusion

Two new N-functionalized 1,4,7-triazacyclononane derivatives have been prepared and, together with the dimethylated derivative of tacn, have been used to prepare dihydroxo-bridged complexes of $[LCu(\mu_2\text{-}OH)_2CuL]^{2+}$. Two of these complexes adopt roof-shaped $[Cu_2(\mu_2\text{-}OH)_2]^{2+}$ cores and, unexpectedly, were found to exhibit ferromagnetic coupling between the two copper(II) centers. Such ferromagnetic coupling has been previously observed in only one tacn derivative, which was proposed to have μ-oxo−μ-aqua bridges between Cu(II) centers, $[Cu_2(\mu_2\text{-}OH_2)(\mu_2\text{-}O)]^{2+}$.[10] The complexes were shown to effectively hydrolyze phosphate esters, with the complex of the benzonitrile derivative showing the highest rate of BNPP cleavage reported so far for a mononuclear Cu(II)−tacn complex.

Scheme 3. Mechanism for the Cleavage of BNPP by Cu−tacn Complexes[5]

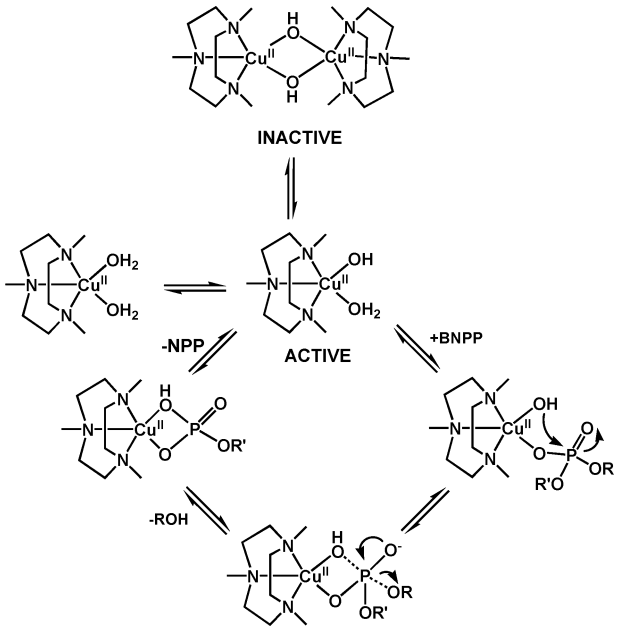

Acknowledgment. This work was supported by the Australian Research Council. M.J.B. was the recipient of an Australian Postgraduate Award.

Supporting Information Available: Details of crystal structure determinations in CIF format. This material is available free of charge via the Internet at http://pubs.acs.org.

IC051983+